

ON THE USE OF RIGID BODY MODES IN THE DEFLATED
PRECONDITIONED CONJUGATE GRADIENT METHOD*

T. B. JÖNSTHÖVEL†, M. B. VAN GIJZEN‡, C. VUIK‡, AND A. SCARPAS†

Abstract. Large discontinuities in material properties, such as those encountered in composite materials, lead to ill-conditioned systems of linear equations. These discontinuities give rise to small eigenvalues that may negatively affect the convergence of iterative solution methods such as the preconditioned conjugate gradient method. This paper considers the deflated preconditioned conjugate gradient method for solving such systems. Our deflation technique uses as the deflation space the rigid body modes of sets of elements with homogeneous material properties. We show that in the deflated spectrum the small eigenvalues are mapped to zero and no longer negatively affect the convergence. We justify our approach through mathematical analysis and show with numerical experiments on both academic and realistic test problems that the convergence of our DPCG method is independent of discontinuities in the material properties.

Key words. deflation, preconditioners, conjugate gradients, rigid body modes, CT scan, structural mechanics

AMS subject classifications. 65F10, 65F08, 65Z05

DOI. 10.1137/100803651

1. Introduction. In many real life engineering applications composite materials play an important role. Good examples are the infrastructural materials found in civil engineering or rock formations in geotechnical engineering. Understanding the interaction between the different components in these materials may lead to more accurate and realistic simulations that are used in the design of more sustainable materials or the displacement of subsurface materials. In recent years there has been a shift in length scales, going from macro- to microscale structural analysis of composite materials. The computationally most demanding task of the finite element (FE) analysis is the solution of large symmetric, positive definite linear systems.

In our application, the composite materials display large differences in the material properties of its components, leading to large jumps in the entries of the stiffness matrix and to ill-conditioned linear systems. In [8], we have studied the relation between these jumps and the deterioration of the performance of the preconditioned conjugate gradient (PCG) method. Specifically, we have shown that there is a correlation between the number of rigid body modes of subbodies of materials contained within the FE mesh and the number of small eigenvalues of the stiffness matrix. Based on this observation, we used rigid body modes combined with existing deflation techniques to remove those small eigenvalues from the spectrum of the stiffness matrix. We introduced the deflated preconditioned conjugate gradient (DPCG) method that uses deflation vectors based on the rigid body modes of sets of elements with similar material properties.

*Submitted to the journal's Computational Methods in Science and Engineering section July 26, 2010; accepted for publication (in revised form) September 11, 2012; published electronically February 11, 2013.

<http://www.siam.org/journals/sisc/35-1/80365.html>

†Faculty of Civil Engineering, Department of Structural Mechanics, Delft University of Technology, 2628CN Delft, The Netherlands (t.b.jonsthovel@tudelft.nl, a.scarpas@tudelft.nl).

‡Faculty of Information Technology and Systems, Department of Applied Mathematical Analysis, Delft University of Technology, 2628CN Delft, The Netherlands (m.b.vangijzen@tudelft.nl, c.vuik@tudelft.nl).

Deflation based preconditioners were first introduced in [14] and have successfully been applied within the field of computational fluid dynamics, with excellent results on problems with discontinuous jumps in coefficients [16], [5], [15]. Rigid body mode deflation generalizes the previous deflation techniques in the sense that it can be applied to discretized coupled partial differential equations.

We note that the idea of using rigid body modes to speed up computations has been widely used in algebraic multigrid methods [18], [7] and the FETI framework [12], [11]. Using rigid body modes based on the underlying geometry of the physical problem in a deflation technique is, to the best of our knowledge, new.

In [9] we compared the parallel implementation of our DPCG method with smoothed aggregated algebraic multigrid, which is currently the state-of-the-art solver for the type of problems considered in this research. Numerical experiments showed that our approach is quite competitive.

In the present paper we provide a mathematical analysis of the rigid body mode deflation. This analysis allows us to formulate rigid body mode deflation in a recursive way, which leads to a natural extension of the technique for composite materials with more than two components. We illustrate our results on both academic test problems and realistic test problems derived from CT scans of a core of asphalt concrete.

2. Problem definition: Composite materials. The majority of FE simulations of composite materials were performed by means of homogenization techniques [4] because these simulations put less strain on CPU time and available computational resources. However, by using homogenization techniques one loses insight into the interaction between the components of the composite materials.

In this application we consider asphalt concrete as composite material. It consists of a mixture of bitumen, stones (also referred to as aggregates), and air voids.

We use the computational framework described in [4] to simulate the component interaction using FE analysis. The resulting stiffness matrix and the corresponding linear system is represented by (1),

$$(1) \quad Ku = f.$$

In the introduction we have argued that solving (1) is the most expensive computation in the FE simulation. In (1) the displacements of the nodes and the differences between the internal and external forces are represented by u and f , respectively. The stiffness matrix K is symmetric positive definite for elastic, constrained systems. We refer the reader to [9] for a more detailed problem definition.

3. On theory of DPCG.

3.1. Motivation of rigid body mode deflation. In [8] we concluded that the number of aggregates times the number of rigid body modes per aggregate (6 in three dimensions) is equal to the number of small eigenvalues of stiffness matrix K . As a result the performance of PCG depends explicitly on the number of aggregates in the composite as well as on the size of Young's moduli. Increasing the number of aggregates introduces correspondingly more (clustered) small eigenvalues in stiffness matrix K . The jumps in Young's moduli are related to the size of the small eigenvalues. We know from [17] that the smallest eigenvalues correspond to the slowly converging components of the solution.

We have argued in [9] that subsets of unconstrained finite elements can be considered as rigid bodies. In our application of asphaltic materials, the aggregates are subsets of elements where Young's modulus binds the elements as a shared property.

3.2. Recursively deflated PCG. In order to define the deflation preconditioner we split the solution of (1) into two parts [5],

$$(2) \quad u = (I - P^T) u + P^T u,$$

in which the project matrix P is defined by

$$(3) \quad P = I - KZ(Z^T K Z)^{-1} Z^T, \quad Z \in \mathbb{R}^{n \times m}.$$

Here $\text{span}(Z)$ is the deflation subspace, i.e., the space to be projected out of the system, and I is the identity matrix of appropriate size. We assume that $m \ll n$ and Z has rank m , which implies that $E \equiv Z^T K Z$ is symmetric positive definite and may be easily computed and factored. Hence,

$$(4) \quad (I - P^T) u = ZE^{-1}Z^T K u = ZE^{-1}Z^T f$$

can be computed immediately. We need only compute $P^T u$. Because KP^T is symmetric,

$$(5) \quad KP^T = PK,$$

we solve the deflated system,

$$(6) \quad PK\hat{u} = Pf$$

for \hat{u} using the CG method and multiply the result by P^T . System (6) is singular and, hence, does not have a unique solution. The projected solution, $u = ZE^{-1}Z^T f + P^T \hat{u}$, however, is unique. The nullspace of PK is explicitly projected out of the solution of the singular system that is computed by CG. We remark that CG can be applied to find a solution of a consistent singular system as is explained in [10], [18].

The definition of P given by (3) does not provide insight into the effect of individual deflation vectors on the spectrum of PK . The next theorem defines a recursive deflation operator which can be used for more extensive eigenvalue analysis of PK . Moreover, it will justify our choice of deflation vectors on which we elaborate later.

DEFINITION 3.1. $P^{(k)} = I - KZ_k(Z_k^T K Z_k)^{-1} Z_k^T$ with $Z_k = [\tilde{Z}_1, \tilde{Z}_2, \dots, \tilde{Z}_k]$, where $\tilde{Z}_j \in \mathbb{R}^{n \times l_j}$ and has rank l_j .

THEOREM 3.2. Let $P^{(k)}$ and Z_k be as in Definition 3.1; then $P^{(k)}K = P_k P_{k-1} \dots P_1 K$, where $P_{i+1} = I - \tilde{K}_i \tilde{Z}_{i+1} (\tilde{Z}_{i+1}^T \tilde{K}_i \tilde{Z}_{i+1})^{-1} \tilde{Z}_{i+1}^T$, $\tilde{K}_i = P_i \tilde{K}_{i-1}$, $\tilde{K}_1 = P_1 K$, $\tilde{K}_0 = K$, $\tilde{Z}_i^T \tilde{K}_{i-1} \tilde{Z}_i^T$, and $Z_i^T K Z_i$ are nonsingular because Z_i are of full rank and K is a symmetric positive definite matrix.

Proof. By induction,

- (i) show $P_1 K = P^{(1)} K$, where $Z_1 = \tilde{Z}_1 \in \mathbb{R}^{n \times l_1}$,
- (ii) assume $P_{i-1} \tilde{K}_{i-2} = \tilde{K}_{i-1} = P^{(i-1)} K$, where $Z_{i-1} = [\tilde{Z}_{i-1}, \tilde{Z}_{i-2}, \dots, \tilde{Z}_1]$, show that $P_i \tilde{K}_{i-1} = P^{(i)} K$, where $Z_i = [\tilde{Z}_i, Z_{i-1}]$, $Z_{i-1} \in \mathbb{R}^{n \times l(i-1)}$, $\tilde{Z}_i \in \mathbb{R}^{n \times l_i}$, and $l = \sum_{r=i}^i l_r$.

For the start of the induction we have to prove (i). The induction hypothesis is given by (ii). We first show that $P_1 K = P^{(1)} K$,

$$\begin{aligned} P_1 K &= K - K \tilde{Z}_1 (\tilde{Z}_1^T K \tilde{Z}_1)^{-1} \tilde{Z}_1^T K \\ &= K - K Z_1 (Z_1^T K Z_1)^{-1} Z_1^T K \\ &= P^{(1)} K, \end{aligned}$$

which implies that (i) is proved. For (ii) we assume $P_{i-1}\tilde{K}_{i-2} = P^{(i-1)}K$, and we prove that this implies $P_i\tilde{K}_{i-1} = P^{(i)}K$,

$$\begin{aligned} P^{(i)}K &= K - KZ_i(Z_i^T K Z_i)^{-1} Z_i^T K \\ &= K - \begin{bmatrix} KZ_{i-1} & K\tilde{Z}_i \end{bmatrix} \left(\begin{bmatrix} Z_{i-1}^T \\ \tilde{Z}_i^T \end{bmatrix} \begin{bmatrix} KZ_{i-1} & K\tilde{Z}_i \end{bmatrix} \right)^{-1} \begin{bmatrix} Z_{i-1}^T K \\ \tilde{Z}_i^T K \end{bmatrix} \\ (7) \quad &= K - \begin{bmatrix} KZ_{i-1} & K\tilde{Z}_i \end{bmatrix} E^{-1} \begin{bmatrix} Z_{i-1}^T K \\ \tilde{Z}_i^T K \end{bmatrix}, \end{aligned}$$

where

$$E = \begin{bmatrix} Z_{i-1}^T K Z_{i-1} & Z_{i-1}^T K \tilde{Z}_i \\ \tilde{Z}_i^T K Z_{i-1} & \tilde{Z}_i^T K \tilde{Z}_i \end{bmatrix}.$$

The matrix $E = \begin{bmatrix} E_{11} & E_{12} \\ E_{21} & E_{22} \end{bmatrix}$ is a symmetric 2×2 block matrix. Its inverse is defined as follows [13]:

$$E^{-1} = \begin{bmatrix} E_{11}^{-1} + E_{11}^{-1} E_{12} (E_{22} - E_{21} E_{11}^{-1} E_{12})^{-1} E_{21} E_{11}^{-1} & -E_{11}^{-1} E_{12} (E_{22} - E_{21} E_{11}^{-1} E_{12})^{-1} \\ -(E_{22} - E_{21} E_{11}^{-1} E_{12})^{-1} E_{21} E_{11}^{-1} & (E_{22} - E_{21} E_{11}^{-1} E_{12})^{-1} \end{bmatrix},$$

with

$$\Psi = \tilde{Z}_i^T K \tilde{Z}_i - \tilde{Z}_i^T K Z_{i-1} (Z_{i-1}^T K Z_{i-1})^{-1} Z_{i-1}^T K \tilde{Z}_i.$$

It follows that

$$\begin{aligned} (E^{-1})_{11} &= (Z_{i-1}^T K Z_{i-1})^{-1} + (Z_{i-1}^T K Z_{i-1})^{-1} Z_{i-1}^T K \tilde{Z}_i \Psi^{-1} \tilde{Z}_i^T K Z_{i-1} (Z_{i-1}^T K Z_{i-1})^{-1}, \\ (E^{-1})_{12} &= - (Z_{i-1}^T K Z_{i-1})^{-1} Z_{i-1}^T K \tilde{Z}_i \Psi^{-1}, \\ (E^{-1})_{21} &= -\Psi^{-1} \tilde{Z}_i^T K Z_{i-1} (Z_{i-1}^T K Z_{i-1})^{-1}, \\ (E^{-1})_{22} &= \Psi^{-1}. \end{aligned}$$

Substitution of these expressions into (7), leads to

$$\begin{aligned} P^{(i)}K &= K - \begin{bmatrix} KZ_{i-1} & K\tilde{Z}_i \end{bmatrix} \begin{bmatrix} (E^{-1})_{11} Z_{i-1}^T K + (E^{-1})_{12} \tilde{Z}_i^T K \\ (E^{-1})_{21} Z_{i-1}^T K + (E^{-1})_{22} \tilde{Z}_i^T K \end{bmatrix} \\ &= K - \left[KZ_{i-1} E_{11}^{-1} Z_{i-1}^T K + KZ_{i-1} E_{12}^{-1} \tilde{Z}_i^T K + K\tilde{Z}_i E_{21}^{-1} Z_{i-1}^T K + K\tilde{Z}_i E_{22}^{-1} \tilde{Z}_i^T K \right] \\ (8) \quad &= K - KZ_{i-1} (Z_{i-1}^T K Z_{i-1})^{-1} Z_{i-1}^T K \\ &\quad - KZ_{i-1} (Z_{i-1}^T K Z_{i-1})^{-1} Z_{i-1}^T K \tilde{Z}_i \Psi^{-1} \tilde{Z}_i^T K Z_{i-1} (Z_{i-1}^T K Z_{i-1})^{-1} Z_{i-1}^T K \\ &\quad + KZ_{i-1} (Z_{i-1}^T K Z_{i-1})^{-1} Z_{i-1}^T K \tilde{Z}_i \Psi^{-1} \tilde{Z}_i^T K \\ &\quad + K\tilde{Z}_i \Psi^{-1} \tilde{Z}_i^T K Z_{i-1} (Z_{i-1}^T K Z_{i-1})^{-1} Z_{i-1}^T K \\ &\quad - K\tilde{Z}_i \Psi^{-1} \tilde{Z}_i^T K. \end{aligned}$$

In order to show $P_i \tilde{K}_{i-1} = P^{(i)} K$ we now elaborate $P_i \tilde{K}_{i-1}$,

$$\begin{aligned}
P_i \tilde{K}_{i-1} &= \tilde{K}_{i-1} - \tilde{K}_{i-1} \tilde{Z}_i \left(\tilde{Z}_i^T \tilde{K}_{i-1} \tilde{Z}_i \right)^{-1} \tilde{Z}_i^T \tilde{K}_{i-1} \\
&= P^{(i-1)} K - P^{(i-1)} K \tilde{Z}_i \left(\tilde{Z}_i^T P^{(i-1)} K \tilde{Z}_i \right)^{-1} \tilde{Z}_i^T P^{(i-1)} K \\
&= K - K Z_{i-1} \left(Z_{i-1}^T K Z_{i-1} \right)^{-1} Z_{i-1}^T K \\
&\quad - \left(K - K Z_{i-1} \left(Z_{i-1}^T K Z_{i-1} \right)^{-1} Z_{i-1}^T K \right) \tilde{Z}_i \\
&\quad \cdot \left(\tilde{Z}_i^T \left(K - K Z_{i-1} \left(Z_{i-1}^T K Z_{i-1} \right)^{-1} Z_{i-1}^T K \right) \tilde{Z}_i \right)^{-1} \\
&\quad \cdot \tilde{Z}_i^T \left(K - K Z_{i-1} \left(Z_{i-1}^T K Z_{i-1} \right)^{-1} Z_{i-1}^T K \right) \\
&= K - K Z_{i-1} \left(Z_{i-1}^T K Z_{i-1} \right)^{-1} Z_{i-1}^T K \\
&\quad - \left(K \tilde{Z}_i - K Z_{i-1} \left(Z_{i-1}^T K Z_{i-1} \right)^{-1} Z_{i-1}^T K \tilde{Z}_i \right) \cdot \Psi^{-1} \\
&\quad \cdot \left(\tilde{Z}_i^T K - \tilde{Z}_i^T K Z_{i-1} \left(Z_{i-1}^T K Z_{i-1} \right)^{-1} Z_{i-1}^T K \right) \\
(9) \quad &= K - K Z_{i-1} \left(Z_{i-1}^T K Z_{i-1} \right)^{-1} Z_{i-1}^T K \\
&\quad - K Z_{i-1} \left(Z_{i-1}^T K Z_{i-1} \right)^{-1} Z_{i-1}^T K \tilde{Z}_i \Psi^{-1} \tilde{Z}_i^T K Z_{i-1} \left(Z_{i-1}^T K Z_{i-1} \right)^{-1} Z_{i-1}^T K \\
&\quad + K Z_{i-1} \left(Z_{i-1}^T K Z_{i-1} \right)^{-1} Z_{i-1}^T K \tilde{Z}_i \Psi^{-1} \tilde{Z}_i^T K \\
&\quad + K \tilde{Z}_i \Psi^{-1} \tilde{Z}_i^T K Z_{i-1} \left(Z_{i-1}^T K Z_{i-1} \right)^{-1} Z_{i-1}^T K \\
&\quad - K \tilde{Z}_i \Psi^{-1} \tilde{Z}_i^T K.
\end{aligned}$$

Note that (8) and (9) are identical, so $P_i \tilde{K}_{i-1} = P^{(i)} K$. \square

Theorem 3.2 provides us with a theoretical framework in which we construct the deflation vectors. We will see that by subsequently adding rigid body modes of particular sets of elements to the deflation space the number of small eigenvalues of the deflated system is smaller compared to the nondeflated system.

3.3. Condition numbers of deflated matrices. Let us denote the i th eigenvalue of K in nondecreasing order by $\lambda_i(K)$ or simply by λ_i . Theorem 10.2.6 in [6] provides a bound on the error of CG. After k iterations of the CG method, the error is bounded by

$$\|u - u_k\|_K \leq 2\|u - u_0\|_K \left(\frac{\sqrt{\kappa} - 1}{\sqrt{\kappa} + 1} \right)^k,$$

where $\kappa = \kappa(K) = \frac{\lambda_n}{\lambda_1}$ is the spectral condition number of K , and the K -norm of u is given by $\|u\|_K = \sqrt{u^T K u}$.

For a positive semidefinite matrix K the condition number should be replaced by the effective condition number [17] that is defined by

$$(10) \quad \kappa_{\text{eff}}(K) = \frac{\lambda_n}{\lambda_{m+1}},$$

in which λ_{m+1} is the smallest nonzero eigenvalue.

Theorem 2.2 from [5], here repeated as Theorem 3.3, implies that a bound on the condition number of $P^{(k)} K$ can be obtained.

THEOREM 3.3. *Let $P^{(k)}$ as defined in Definition 3.1 and suppose there exists a splitting $K = C + R$ such that C and R are symmetric positive semidefinite with $\mathcal{N}(C) = \text{span}\{Z_k\}$, the nullspace of C . Then for ordered eigenvalues λ_i ,*

$$(11) \quad \lambda_i(C) \leq \lambda_i(P^{(k)}K) \leq \lambda_i(C) + \lambda_{\max}(P^{(k)}R).$$

Moreover, the effective condition number of $P^{(k)}K$ is bounded by

$$(12) \quad \kappa_{\text{eff}}(P^{(k)}K) \leq \frac{\lambda_n(K)}{\lambda_{m+1}(C)}.$$

Proof. See [5, p. 445] for the proof. \square

We use deflation in combination with conventional preconditioner techniques such that we can treat the smallest as well as the largest eigenvalues. For a preconditioned deflated matrix $L^{-1}P^{(k)}KL^{-T}$, with $M = LL^T$ the preconditioner, the bound in Theorem 3.3 becomes

$$(13) \quad \kappa_{\text{eff}}(L^{-1}P^{(k)}KL^{-T}) \leq \frac{\lambda_n(L^{-1}KL^{-T})}{\lambda_{m+1}(L^{-1}CL^{-T})}.$$

4. Recursive deflation for FE problems.

4.1. Recursive deflation strategy. In this section we introduce a strategy to construct the deflation space Z_j for $P^{(j)}K$ of Definition 3.1 to obtain decoupled problems using Theorems 3.3 and 3.2. We start by observing that nullspaces of sets of elements are represented by the rigid body modes of those sets of elements. By choosing sets of elements we define C and the nullspace of C is our deflation space, which is by definition spanned by the rigid body modes. In the appendix an algorithm is given for computing rigid body modes of sets of elements.

We have an arbitrary FE mesh Ω consisting of elements e_i , $i = 1, \dots, n$, and m materials, sorted by decreasing stiffness. We will elaborate on the importance of the ordering by material stiffness in section 4.2. Material j of the FE mesh can have multiple bodies j_k which is the collection of connected elements that share the same material property. We note that each body of material induces a jump in the entries of the stiffness matrix of which the size depends on the differences in stiffness of the corresponding materials. Hence it is important to distinguish all bodies of all materials as we want to decouple those regions in the stiffness matrix. The set of elements that makes up a body l of the material j is defined as Ω_j^l , where $\Omega = \bigcup_{j=1}^m \{\bigcup_{l=1}^{j_k} \Omega_j^l\}$. Let $\mathcal{I} = \{i : e_i \subset \Omega\}$ be defined as the index set of Ω . The index set of Ω_j^l is $\mathcal{I}_j^l = \{i : e_i \subset \Omega_j^l\}$. We also define index set $\mathcal{I}_j^{l,\Gamma} = \{i : (e_i \subset \Omega \setminus \Omega_j^l) \wedge (e_i \cap e_k \neq \emptyset \forall e_k \subset \Omega_j^l)\}$, which contains all indices of the elements of $\Omega \setminus \Omega_j^l$ that are connected to (the boundary elements of) Ω_j^l .

Start with material $j = 1$ and body $l = 1$, which corresponds to submesh Ω_1^1 . This yields the first splitting:

$$\begin{aligned} \tilde{K}_0 &= A = C_0 + R_0, \\ C_0 &= \sum_{i \in \mathcal{I}_1^1} N_{e_i}^T K_{e_i} N_{e_i} + \sum_{i \in \mathcal{I} \setminus \{\mathcal{I}_1^{1,\Gamma} \cup \mathcal{I}_1^1\}} N_{e_i}^T K_{e_i} N_{e_i}, \\ R_0 &= \sum_{i \in \mathcal{I}_1^{1,\Gamma}} N_{e_i}^T K_{e_i} N_{e_i}. \end{aligned}$$

The matrix C_0 consists of the assembly of all finite elements that belong to body $l = 1$ of material $j = 1$. Matrix K_{e_i} is the element stiffness matrix of element e_i with corresponding connectivity matrix N_{e_i} . The matrix R_0 consists of the assembly of all finite elements that share nodes with the elements on the boundary of body $l = 1$ of material $j = 1$ but that are not contained within submesh Ω_1^1 . The first splitting yields $\mathcal{N}(C_0) = \tilde{Z}_1$ and $P_1 = I - \tilde{A}_0 \tilde{Z}_1 (\tilde{Z}_1^T \tilde{A}_0 \tilde{Z}_1)^{-1} \tilde{Z}_1^T$. By this splitting we have decoupled the first body of material 1 from all other materials. The rigid body modes of all elements corresponding to the first body of material 1 are contained in $\mathcal{N}(C_0)$. We construct $\tilde{A}_1 = P_1 A = P_1(C_0 + R_0) = P_1 C_0 + P_1 R_0 = C_0 + \tilde{R}_0$, where $P_1 C_0 = C_0$ follows by definition of P_1 . Continuing with the second body of material 1 and repeating the previous decoupling step gives

$$\begin{aligned}\tilde{K}_1 &= P_1 A = C_0 + \tilde{R}_0 = C_1 + R_1 + \tilde{R}_0, \\ C_1 &= \sum_{i \in \mathcal{I}_1^1} N_{e_i}^T K_{e_i} N_{e_i} + \sum_{i \in \mathcal{I}_1^2 \setminus \mathcal{I}_1^{1,\Gamma}} N_{e_i}^T K_{e_i} N_{e_i} + \sum_{i \in \mathcal{I} \setminus \bigcup_{l=1}^2 \{\mathcal{I}_1^{l,\Gamma} \cup \mathcal{I}_1^l\}} N_{e_i}^T K_{e_i} N_{e_i}, \\ R_1 &= \sum_{i \in \mathcal{I}_1^{2,\Gamma} \setminus \mathcal{I}_1^{1,\Gamma}} N_{e_i}^T K_{e_i} N_{e_i}.\end{aligned}$$

Hence, $\mathcal{N}(C_1) = \tilde{Z}_2$ and $P_2 = I - \tilde{A}_1 \tilde{Z}_2 (\tilde{Z}_2^T \tilde{A}_1 \tilde{Z}_2)^{-1} \tilde{Z}_2^T$. Continue for all bodies and materials. At splitting $m = \sum_{j=1}^{n-1} j_k + l$ for material n and body l ,

$$\begin{aligned}\tilde{K}_{m-1} &= C_{m-2} + \tilde{R}_{m-2} = C_{m-1} + R_{m-1} + \tilde{R}_{m-2}, \\ C_{m-1} &= \sum_{q=1}^{n-1} \left[\sum_{r=1}^{j_k} \left[\sum_{i \in \mathcal{P}} N_{e_i}^T K_{e_i} N_{e_i} \right] \right] \\ &\quad + \sum_{r=1}^l \left[\sum_{i \in \mathcal{C}} N_{e_i}^T K_{e_i} N_{e_i} \right] \\ &\quad + \sum_{i \in \mathcal{U}} N_{e_i}^T K_{e_i} N_{e_i}, \\ R_{m-1} &= \sum_{i \in \mathcal{B}} N_{e_i}^T K_{e_i} N_{e_i},\end{aligned}$$

where

$$\begin{aligned}\mathcal{P} &= \mathcal{I}_q^r \setminus \left\{ \bigcup_{j=1}^{q-1} \bigcup_{s=1}^{j_k} \mathcal{I}_j^{s,\Gamma} \right\}, \\ \mathcal{C} &= \mathcal{I}_n^r \setminus \left\{ \bigcup_{j=1}^{n-1} \bigcup_{s=1}^{j_k} \mathcal{I}_j^{s,\Gamma} \right\} \cup \left\{ \bigcup_{s=1}^{l-1} \mathcal{I}_n^{s,\Gamma} \right\}, \\ \mathcal{U} &= \mathcal{I} \setminus \left\{ \bigcup_{q=1}^{n-1} \left\{ \bigcup_{r=1}^{q_k} \mathcal{I}_q^{r,\Gamma} \cup \mathcal{I}_q^r \right\} \right\} \cup \left\{ \bigcup_{r=1}^l \mathcal{I}_n^{r,\Gamma} \cup \mathcal{I}_n^r \right\}, \\ \mathcal{B} &= \mathcal{I}_n^{l,\Gamma} \setminus \left\{ \bigcup_{j=1}^{n-1} \bigcup_{s=1}^{j_k} \mathcal{I}_j^{s,\Gamma} \right\} \cup \left\{ \bigcup_{s=1}^{l-1} \mathcal{I}_n^{s,\Gamma} \right\}.\end{aligned}$$

Hence, $\mathcal{N}(C_{m-1}) = \tilde{Z}_m$ and $P_{m-1} = I - \tilde{K}_{m-1}\tilde{Z}_m(\tilde{Z}_m^T\tilde{K}_{m-1}\tilde{Z}_m)^{-1}\tilde{Z}_m^T = P$ with $P = I - AZ(Z^TAZ)^{-1}Z^T$ and $\text{span}\{Z\} = \bigcup_{j=1}^m \text{span}\{\tilde{Z}_j\}$. The above expression for \tilde{K}_{m-1} is rather complex. We have divided the index sets needed for assembly of C_{m-1} and R_{m-1} into 4 subsets, \mathcal{P} , \mathcal{C} , \mathcal{U} , and \mathcal{B} . The set \mathcal{P} contains all element indices that belong to body r of material q except for all elements that are included in boundary element sets of previously assembled materials and bodies. The set \mathcal{C} contains all the element indices that belong to body r of current material n except for all elements that are included in boundary element sets of previously assembled materials and bodies, and the $l-1$ assembled bodies of the current material. The set \mathcal{U} contains all the element indices that belong to materials and bodies that have not been assembled yet. The set \mathcal{B} contains all element indices that belong to elements that lie against the boundary of body l of current material n but without all elements that are contained within boundary sets of previously assembled bodies and materials.

4.1.1. Illustrative example: One-dimensional (1D) Poisson equation.

The main results of this paper are on three-dimensional (3D) mechanical problems. However, the general deflation theory and strategy provided can be applied to any FE problem. We will illustrate the effect of the deflation operator on the 1D Poisson equation with discontinuous coefficients. For this case deflation is easier to understand and analyze when compared to 3D mechanical problems. The 1D Poisson equation reads

$$(14) \quad -\frac{d}{dx} \left(c(x) \frac{du(x)}{dx} \right) = f(x), \quad x \in [0, l],$$

$$(15) \quad u(0) = 0, \quad \frac{du}{dx}(l) = 0,$$

where $c(x)$ is a given piecewise constant function, $u(x)$ the unknown displacement field, and $f(x)$ the given source term.

We discretize (14) with the FE method using linear first-order shape functions and equally spaced elements of size h . It is well known that in this particular case the FE stencil for the 1D Poisson equation reads

$$(16) \quad \begin{bmatrix} c(x_i) & -c(x_{i+1}) \\ -c(x_i) & c(x_{i+1}) \end{bmatrix}.$$

We introduce an FE mesh for the line $[0, l]$ including three domains $\Omega_1 = \{x_1, \dots, x_4\}$, $\Omega_2 = \{x_5, \dots, x_8\}$, and $\Omega_3 = \{x_9, \dots, x_{13}\}$.

For the sake of simplicity we will write $c_i = c(x_i)$, where $i = 1, \dots, 13$, $x_1 = h$, and $x_{13} = l$. Furthermore because c_i is constant on each material domain we will use $c_i = c_1$, $c_i = c_2$, and $c_i = c_3$ on Ω_1 , Ω_2 , and Ω_3 , respectively.

After discretization we obtain

$$(17) \quad K\mathbf{u} = hf(\mathbf{x}),$$

where

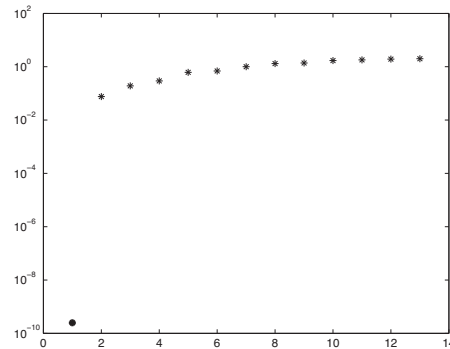
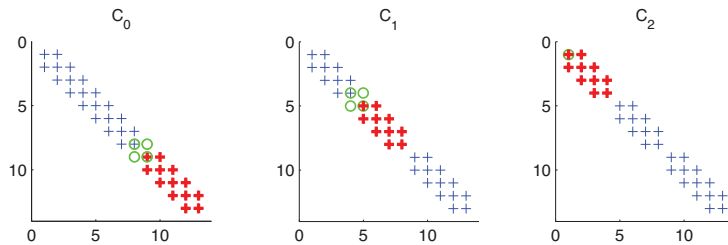
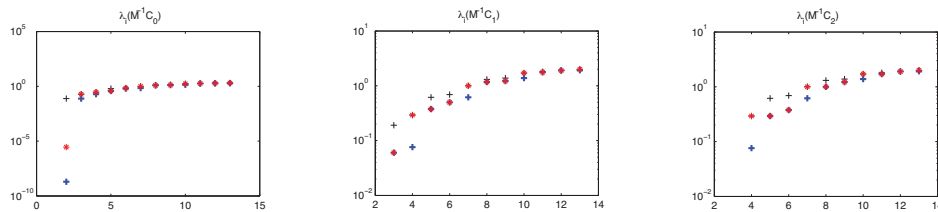
$$K = \frac{1}{h} \begin{bmatrix} 2c_1 & -c_1 & & & & & \\ -c_1 & \ddots & \ddots & & & & \emptyset \\ & \ddots & 2c_1 & -c_1 & & & \\ & & -c_1 & c_1 + c_2 & -c_2 & & \\ & & & -c_2 & \ddots & \ddots & \\ & & & & \ddots & 2c_2 & -c_2 \\ & & & & & -c_2 & c_2 + c_3 & -c_3 \\ & & & & & & -c_3 & \ddots & \ddots \\ \emptyset & & & & & & & \ddots & 2c_3 & -c_3 \\ & & & & & & & & -c_3 & c_3 \end{bmatrix}$$

and $\mathbf{u} = [u_1, u_2, \dots, u_{13}]^T$, $\mathbf{x} = [x_1, x_2, \dots, x_{13}]^T$. The stiffness matrix K of (17) is preconditioned by $M \simeq K$. In this example we take $M = \text{diag}(K)$.

The spectrum of $M^{-1}K$ is given by Figure 1. Clearly the smallest eigenvalue, which is of $\mathcal{O}(10^{-10})$ and induced by the (only real) rigid body contained in the mesh, is much smaller compared to the other eigenvalues. Moreover, it affects the condition number of $M^{-1}K$. Now we apply the deflation strategy by finding a correct splitting of K . We sort the materials in decreasing order of diffusion. Figure 2 shows the sparsity pattern of the three splitting matrices C_0 , C_1 , and C_2 . In matrix C_0 the assembly of the elements belonging to stiffest material 3 is represented by the bold crosses. The interface between weaker materials 2 and 3, which goes to R_0 , is represented by the circles and all other elements are represented by the nonbold crosses. The second splitting is the decoupling of material 2 from the system; again those elements are represented by the bold crosses. The interface between materials 2 and 3 has been removed already, and the interface between materials 2 and 1 goes to R_1 . The remaining splitting is the decoupling of material 1 from the boundary conditions which go to R_2 .

4.2. Deflation vectors in the neighborhood of a jump. If some elements of a less stiff material are assigned to the element set of a stiffer material, the material stiffness matrices are not decoupled. We illustrate this with a simple example. When a node belongs to two elements and two different materials and is assigned to the wrong (least stiff) element with respect to the splitting of K , then by applying the preconditioner the coupling between the stiffness matrices remains. For instance, the 1D Poisson problem and preconditioning based on diagonal scaling, the entry on the main diagonal is $c_1 + c_2$, with $c_1 \ll c_2$. Clearly, when decoupled correctly, we have in splitting of K only c_2 on the main diagonal of C , and hence $M^{-1}C$ gives $\frac{c_2}{c_1+c_2} \approx 1$. With a wrong choice of deflation vectors, we have c_1 on the main diagonal of C , and hence $M^{-1}C$ gives $\frac{c_1}{c_1+c_2} \approx \frac{1}{c_2} \ll 1$. However, all other terms on the diagonal of $M^{-1}C$ will be approximately 1, introducing small eigenvalues for this material and unfavorable local spectrum of eigenvalues of $M^{-1}C$.

4.2.1. Illustrative example: 1D Poisson equation (continued). We illustrate the effect of incorrect decoupling by analyzing the spectrum of the splitting matrices for the 1D Poisson equation. Figure 3 shows the spectrum of $M^{-1}C_i$ for the correct (star) and wrong (bold cross) choice of deflation vectors compared to the spectrum of $M^{-1}K$. After applying three deflation operations, we observe from the

FIG. 1. Spectrum of $M^{-1}K$ where $[c_1, c_2, c_3] = [1, 10^4, 10^8]$.FIG. 2. Sparsity pattern C_0 , C_1 , and C_2 . Nonzero elements represented by symbols; corresponding to deflated material, interface elements and remaining elements pictured by bold crosses, circles, and nonbold crosses, respectively.FIG. 3. Spectrum of $M^{-1}C_i$ (\star correct, $+$ wrong choice deflation vectors) compared to spectrum of $M^{-1}K$ ($+$).

spectrum of $M^{-1}C_2$ that the smallest eigenvalue of the wrong choice of deflation vectors is much smaller than the smallest eigenvalue for the correct choice of deflation vectors, which coincides with the smallest eigenvalue in the spectrum of $M^{-1}K$. Moreover, we can see from the spectrum of C_0 and C_1 that the wrong choice has clearly been made with respect to coupling of material 3 and material 2. The effective condition number of the wrong choice of deflation vectors will affect the performance of DPCG. Figure 4 shows the convergence of the error of DPCG and PCG for correct

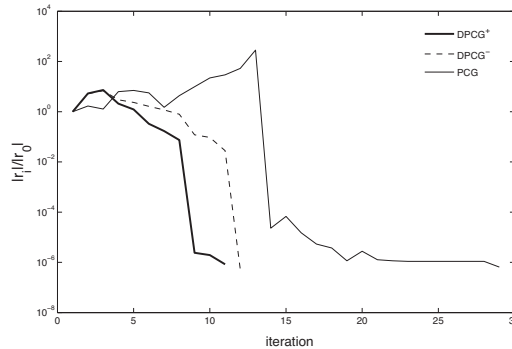


FIG. 4. Convergence of DPCG and PCG where $[c_1, c_2, c_3] = [1, 10^4, 10^8]$ and $DPCG^+$, $DPCG^-$ represent the correct and wrong choice of deflation vectors, respectively.

Algorithm 1. DP CG solving $K\mathbf{u} = \mathbf{f}$.

```

Select  $\mathbf{u}_0$ . Compute  $\mathbf{r}_0 = (\mathbf{f} - K\mathbf{u}_0)$ , set  $\hat{\mathbf{r}}_0 = P\mathbf{r}_0$ , and  $\mathbf{p}_0 = \hat{\mathbf{r}}_0$ 
Solve  $M\mathbf{y}_0 = \hat{\mathbf{r}}_0$  and set  $\mathbf{p}_0 = \mathbf{y}_0$ 
for  $j = 0, 1, \dots$  until convergence do
     $\hat{\mathbf{w}}_j = PK\mathbf{p}_j$ ,
     $\alpha_j = \frac{(\hat{\mathbf{r}}_j, \mathbf{y}_j)}{(\hat{\mathbf{w}}_j, \mathbf{p}_j)}$ ,
     $\hat{\mathbf{u}}_{j+1} = \hat{\mathbf{u}}_j + \alpha_j \mathbf{p}_j$ ,
     $\hat{\mathbf{r}}_{j+1} = \hat{\mathbf{r}}_j - \alpha_j \hat{\mathbf{w}}_j$ ,
    Solve  $M\mathbf{y}_{j+1} = \hat{\mathbf{r}}_{j+1}$ ,
     $\beta_j = \frac{(\hat{\mathbf{r}}_{j+1}, \mathbf{y}_{j+1})}{(\hat{\mathbf{r}}_j, \mathbf{y}_j)}$ ,
     $\mathbf{p}_{j+1} = \mathbf{y}_{j+1} + \beta_j \mathbf{p}_j$ ,
end for
 $\mathbf{u} = ZE^{-1}Z^T\mathbf{f} + P^T\hat{\mathbf{u}}_{j+1}$ 

```

(+) and wrong (-) choice of deflation vectors. The performance of $DPCG^-$ is worse than $DPCG^+$, as predicted by values of the eigenvalues in Figure 3.

4.3. DPCG algorithm. The deflation method was proposed by [14]. A practical variant of the deflated preconditioned gradient method from [16] is given by Algorithm 1.

We determine the computational cost of DPCG compared to PCG. The projector P is never computed explicitly. We compute the sparse matrix $K_Z = KZ$ as well as the inverse of the small dense matrix $E = Z^T K_Z$ beforehand. Assume the (full rank) deflation space has dimension $d \ll n$ where $K \in \mathcal{R}^{n \times n}$, implying $Z \in \mathcal{R}^{n \times d}$, $E \in \mathcal{R}^{d \times d}$, and $K_Z \in \mathcal{R}^{n \times d}$. Evaluation of $w = Pv$ is equal to $w = v - K_Z E^{-1} Z^T v$. Stiffness matrix K , deflation vectors Z , and matrix K_Z are sparse. We compare the cost of one matrix vector product of the stiffness matrix K and the deflation matrix P by comparing the number of flops. Assume that the average number of nonzeros for each row of K , Z^T , and K_Z is α , β , and γ , respectively. The total number of flops of one matrix vector multiplication with stiffness matrix K is $2\alpha n$. The (cumulative) number of flops of P is $(2\beta d) + (2d^2) + (2\gamma n) + n$; clearly $2\gamma n$ is the dominating term but is difficult to estimate as γ depends on the number of deflation vectors. However, if the number of deflation vectors is small and Z very sparse, the number of nonzeros

in K_Z will be comparable to the number of nonzeros of K , and the number of flops of both operators will be of the same order of magnitude. Choosing dense deflation vectors with much overlap may cause operator P to be more expensive than K in terms of flops.

5. Numerical experiments. Both experiments in this section concern the analysis of asphaltic materials subjected to an external force. These materials give rise to coupled partial differential equations [4]. The experiments make use of the same set of material parameters. We distinguish between three materials: aggregates, bitumen, and air voids. The corresponding stiffness coefficients (E modulus) are given in Table 1 and are the dominating contributions to the entries of the stiffness matrix. In order to illustrate the effect of the discontinuities on the convergence of PCG, we show results for 4 sets of parameters. The first set (i) from Table 1 contains realistic material parameters. The other sets do not have a direct physical meaning to asphaltic materials, but are used for the illustration of the performance of deflation. We have conducted the experiments with two different preconditioners, diagonal scaling, and incomplete Cholesky with a drop tolerance of 10^{-2} . This drop tolerance was determined after performing several tests with ILUPACK [2] and represents the optimal value in terms of memory usage (lower drop tolerance demands more memory) and the speed of the back solve (lower tolerance yields a slower back solve) against the performance of the preconditioner in terms of reduction in number of iterations of DPCG. We have implemented PCG and DPCG into the existing parallel FE software package CAPA-3D [3]. All experiments were done on a cluster of Dell workstations containing eight CPUs Intel Xeon E5450, running at 3.00GHz and connected by Infiniband. We compare the additional storage used by deflation as well as the ILU preconditioner to the storage of stiffness matrix K . In both experiments the additional storage of the deflation operator, i.e., the matrices Z , K_Z , and E^{-1} , is approximately 50% of the storage of the stiffness matrix, and the additional storage of the ILU preconditioner is approximately 150% of the storage of the stiffness matrix.

TABLE 1
E modulus for different materials.

	Aggregate	Bitumen	Air voids
(i)	69000	5000	100
(ii)	690000	5000	100
(iii)	69000	500	100
(iv)	69000	5000	10⁻²

5.1. Experiment 1: Cylinder containing aggregates and bitumen. The case given in Figure 5 is a cylinder of soft material (air voids) containing three aggregates embedded in a layer of bitumen. The mesh contains 1.2×10^4 degrees of freedom. We compare DPCG and PCG in combination with diagonal scaling. The case involves a mixture of materials that is subjected to an external force applied to the upper boundary of the volume. Zero displacement boundary conditions are imposed on the base of the volume; this is homogeneous Dirichlet boundary conditions to all degrees of freedom in the x, z -plane for $y = 0$. We note that the case resembles the uniaxial compression test, which is a standard laboratory test. We observe the convergence behavior of DPCG and PCG for variations in the E modulus of the bitumen and aggregates as given in Table 1. We compare a standard choice for the values of parameter E [4] with increased stiffness of the aggregates, and decreasing

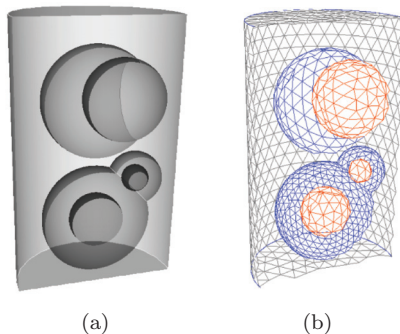


FIG. 5. *FE mesh and schematic representation of cylinder containing three aggregates (red) represented by spheres and surrounded by bitumen (blue) and air voids (black).*

stiffness for the bitumen and air voids. We have identified six rigid bodies and thus have 36 deflation vectors.

Figure 6 shows the convergence of PCG and DPCG for parameter sets (i) to (iv). In Table 2 we provide the CPU wall time and iteration count of PCG and DPCG. Clearly the convergence of the solution with PCG is slow and highly oscillating. PCG compared to DPCG is also slower in terms of CPU time. But due to the small problem size, this is more a qualitative example rather than quantitative. We observe in the plots of sets (i) to (iii) that the value of the material stiffness for the aggregates and bitumen does not influence the number of iterations of DPCG. This is what we expected. The stiffness matrices corresponding to the aggregates and bitumen have been decoupled. The effective condition number is bounded by the smallest eigenvalue of the least stiff material, the air voids. This can also be observed in the plot of set (iv). The number of iterations of DPCG increases from 150 towards 242 for air. As the value of the material stiffness of the air voids changes from 100 to 10^{-2} , the effective condition number increases as well as the number of iterations of both DPCG and PCG. However, this is not surprising as the smallest (nonzero) eigenvalue is determined by the least stiff material, due to the decoupling of the stiffness matrices corresponding to the different materials. When the stiffness decreases, the smallest eigenvalue will become smaller and subsequently the condition number increases. We do not consider this as a shortcoming of the deflation method as it can and must be solved by applying the right preconditioner.

5.2. Experiment 2: FE mesh from CT scan. The case given in Figure 7 is an FE mesh of a real life sample of asphaltic material obtained from CT scan. The mesh contains 2.3×10^5 degrees of freedom. We compare DPCG and PCG in combination with incomplete Cholesky with drop tolerance 10^{-2} . The case involves a mixture of materials that is subjected to an external force applied to the upper boundary of the volume. Zero displacement boundary conditions are imposed on three sides of the volume, which are homogeneous Dirichlet boundary conditions to all degrees of freedom in the x, z -, x, y -, and y, z -planes for $y = 0$, $z = 0$, and $x = 0$, respectively. We observe the convergence behavior of DPCG and PCG for variations in the E modulus of the bitumen and aggregates as given in Table 1. We compare a standard choice of parameters [4] with increased stiffness of the aggregates, and decreasing stiffness for the bitumen.

There is a difference between the artificial cylinder and the sample of real asphaltic

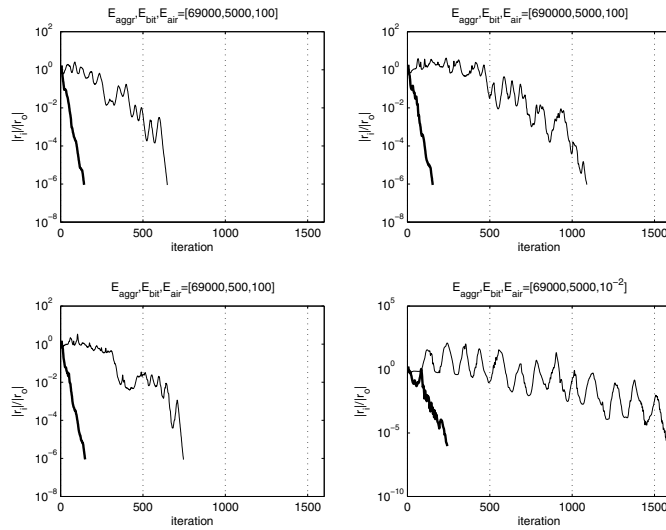


FIG. 6. Convergence of PCG and DPCG (bold line) for cylinder containing three aggregates.

TABLE 2
Example 1: CPU wall time(s) PCG and DPCG.

	PCG		DPCG	
	Iter	cpu(s)	Iter	cpu(s)
(i)	648	0.288	143	0.204
(ii)	1089	0.477	154	0.175
(iii)	746	0.328	149	0.172
(iv)	1581	0.677	242	0.276

material. Where it was possible to decouple all materials in case of the cylinder, for an FE mesh obtained from a CT scan this is much more involved. We can see from Figure 8(b) and (c) that there exist many small bodies of material. Each body is represented in the deflation space by six rigid body modes. However, due to overlap, many of these sparse vectors will become zero, implying a singular deflation matrix. Moreover, because of the large number of small bodies and thus deflation vectors, it would be more favorable in terms of overhead to collapse these bodies into one entity. Therefore, we have used an adapted version of the deflation strategy of section 4.1.1. By combining sets of elements of different materials, we still have a decoupling when we keep in mind the decreasing order of stiffness for the construction of the splitting of Theorem 3.3. We note that we lose some rigid body modes, and hence a worse bound of the condition number for PK but we gain performance because of a large reduction in deflation vectors and avoid singularity of the deflation matrix. Also we have omitted set (iv) from this test because the FE software would not run this value of air voids due to collapsing elements (negative Jacobian). We have identified 27 rigid bodies and, thus, have 162 deflation vectors.

We observe in Figure 9 that PCG has a strongly oscillating path of convergence and DPCG has nearly a straight line. In Table 3 we provide the CPU wall time and iteration count of PCG and DPCG. Clearly the unfavorable eigenvalues have been

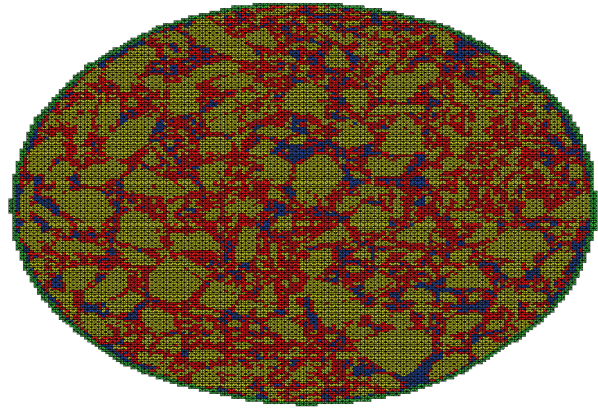


FIG. 7. FE mesh representing core of asphaltic material containing aggregates (yellow), bitumen (red), and air voids (blue).

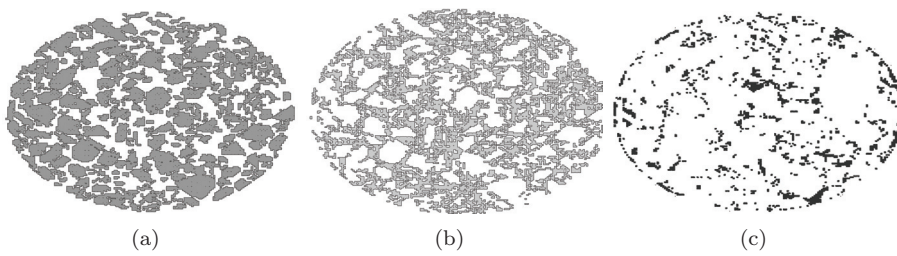


FIG. 8. Deflation strategy, identify sets of elements corresponding to material: (a) aggregates, (b) bitumen, and (c) air voids.

removed by deflation. However, the system is not decoupled completely because the number of iterations is not invariant for different sets of material parameters. But the number of iterations of DPCG is much smaller compared to PCG. The performance of DPCG in terms of CPU wall time is also better compared to PCG.

6. Conclusion. We considered the application of the deflated preconditioned conjugate gradient (DPCG) method to mechanical problems with strongly varying stiffness of materials. We described a simple general applicable way on how to choose deflation vectors by using the rigid body modes of subsets of elements. By combining the deflation technique and the computation of the exact rigid body modes of the components, the robust DPCG is obtained. The DPCG method is insensitive to large jumps in the E modulus of materials. The amount of work per iteration for the deflation operator of DPCG is comparable to one matrix vector product. However, this does not imply that DPCG becomes twice as expensive as PCG because the preconditioning step consumes most resources in both time and memory. For most applications, using sparse deflation vectors, DPCG is roughly 30% more expensive in time per iteration compared to PCG.

Appendix. Computing rigid body modes of a finite element. We know from [1] that the rigid body modes of a finite element are spanned by the kernel base

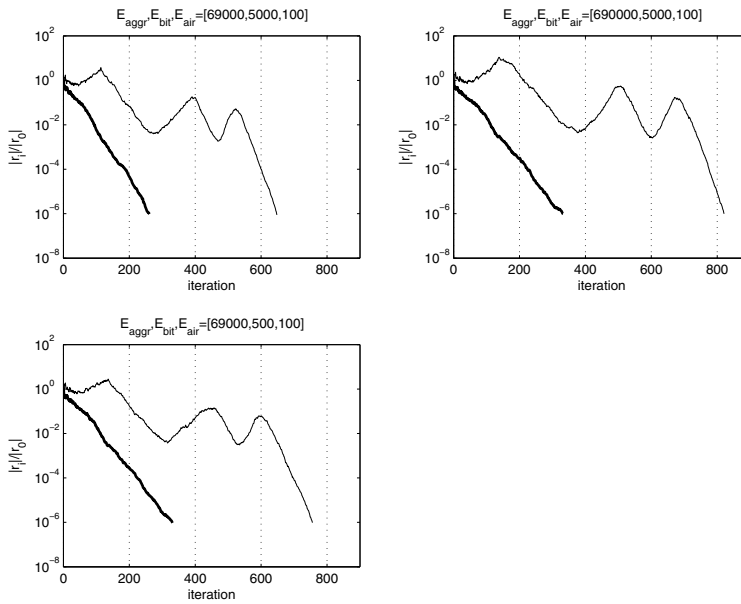


FIG. 9. Convergence of PCG and DPCG for a real slice of asphaltic material.

TABLE 3
Example 2: CPU wall time(s) PCG and DPCG.

	PCG		DPCG	
	Iter	cpu(s)	Iter	cpu(s)
i.	648	13.18	261	7.26
ii.	821	17.48	332	9.31
iii.	756	15.21	331	8.89

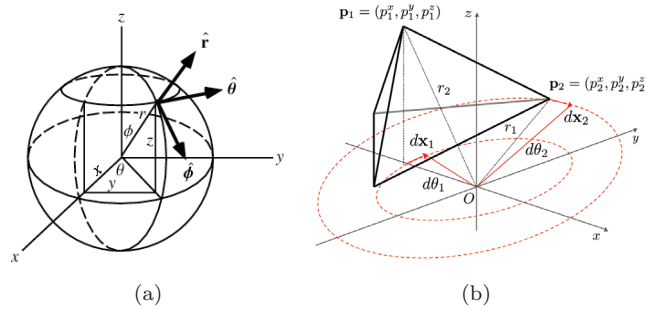
vectors of the corresponding element stiffness matrix. We will show a fast and cheap solution for the computation of the rigid body modes. The same principle can be easily extended to sets of finite elements of arbitrary shape and order. We note that the rigid body modes are only defined by the geometric properties of the element.

In three dimensions a finite element has six rigid body motions: three translations and three rotations. For simplicity we consider a four noded tetrahedral element; however, all derivations can be extended to N noded elements without loss of generality. The coordinate vector of the element is given by

$$\{ \begin{array}{cccccccccc} x_1 & y_1 & z_1 & x_2 & y_2 & z_2 & x_3 & y_3 & z_3 & x_4 & y_4 & z_4 \end{array} \}^T.$$

A translation can be considered as a uniform displacement of every node in a given direction. To obtain three orthogonal translations we choose the x , y , and z directions, respectively. The three translation vectors are given by

$$\begin{aligned} & \{ \begin{array}{cccccccccc} 1 & 0 & 0 & 1 & 0 & 0 & 1 & 0 & 0 & 1 & 0 & 0 \end{array} \}^T, \\ & \{ \begin{array}{cccccccccc} 0 & 1 & 0 & 0 & 1 & 0 & 0 & 1 & 0 & 0 & 1 & 0 \end{array} \}^T, \\ & \{ \begin{array}{cccccccccc} 0 & 0 & 1 & 0 & 0 & 1 & 0 & 0 & 1 & 0 & 0 & 1 \end{array} \}^T. \end{aligned}$$

FIG. 10. (a) *Spherical coordinates*, (b) *rotation around origin of tetrahedral element in x, y -plane*.

The rotations can be easily described using the spherical coordinate system

$$x = r \cos(\theta) \sin(\phi), \quad y = r \sin(\theta) \sin(\phi), \quad z = r \cos(\phi),$$

where

$$r = \sqrt{x^2 + y^2 + z^2}, \quad \theta = \tan^{-1}\left(\frac{y}{x}\right), \quad \phi = \cos^{-1}\left(\frac{x}{r}\right),$$

and θ and ϕ as in Figure 10(a).

We derive a rotation $d\theta$ in the x, y -plane, hence $d\phi = 0$ and $dr = 0$. The x, y , x, z and y, z planes contain unique rotations. The corresponding vectors can be found by swapping axis. For an arbitrary point in space which has spherical coordinates (r, θ, ϕ) a change $d\theta$ in the x, y -plane yields a displacement in Cartesian coordinates of

$$dx = -r \sin(\theta) \sin(\phi) d\theta, \quad dy = r \cos(\theta) \sin(\phi) d\theta, \quad dz = 0.$$

Figure 10(b) shows the rotation for one element with respect to the origin over angle $d\theta$. By using above expressions we obtain all three rotation vectors:

Rotation x, y -plane:

$$\theta_j = \tan^{-1}\left(\frac{y_j}{x_j}\right), \quad \phi_j = \cos^{-1}\left(\frac{z_j}{r_j}\right), \quad \begin{Bmatrix} -r_1 \sin(\theta_1) \sin(\phi_1) \\ r_1 \cos(\theta_1) \sin(\phi_1) \\ 0 \\ -r_2 \sin(\theta_2) \sin(\phi_2) \\ r_2 \cos(\theta_2) \sin(\phi_2) \\ 0 \\ -r_3 \sin(\theta_3) \sin(\phi_3) \\ r_3 \cos(\theta_3) \sin(\phi_3) \\ 0 \\ -r_4 \sin(\theta_4) \sin(\phi_4) \\ r_4 \cos(\theta_4) \sin(\phi_4) \\ 0 \end{Bmatrix}.$$

Rotation y, z -plane:

$$\theta_j = \tan^{-1}\left(\frac{z_j}{x_j}\right), \quad \phi_j = \cos^{-1}\left(\frac{y_j}{r_j}\right), \quad \begin{Bmatrix} -r_1 \sin(\theta_1) \sin(\phi_1) \\ 0 \\ r_1 \cos(\theta_1) \sin(\phi_1) \\ -r_2 \sin(\theta_2) \sin(\phi_2) \\ 0 \\ r_2 \cos(\theta_2) \sin(\phi_2) \\ -r_3 \sin(\theta_3) \sin(\phi_3) \\ 0 \\ r_3 \cos(\theta_3) \sin(\phi_3) \\ -r_4 \sin(\theta_4) \sin(\phi_4) \\ 0 \\ r_4 \cos(\theta_4) \sin(\phi_4) \end{Bmatrix}.$$

Rotation x, z -plane:

$$\theta_j = \tan^{-1} \left(\frac{z_j}{y_j} \right), \quad \phi_j = \cos^{-1} \left(\frac{x_j}{r_j} \right), \quad \left\{ \begin{array}{l} 0 \\ r_1 \cos(\theta_1) \sin(\phi_1) \\ -r_1 \sin(\theta_1) \sin(\phi_1) \\ 0 \\ r_2 \cos(\theta_2) \sin(\phi_2) \\ -r_2 \sin(\theta_2) \sin(\phi_2) \\ 0 \\ r_3 \cos(\theta_3) \sin(\phi_3) \\ -r_3 \sin(\theta_3) \sin(\phi_3) \\ 0 \\ r_4 \cos(\theta_4) \sin(\phi_4) \\ -r_4 \sin(\theta_4) \sin(\phi_4) \end{array} \right\}.$$

We compute the nullspace of each element matrix. Sets of elements make up the bodies of materials, as a collection of elements share a certain property and are neighbors. The rigid body modes of a collection of elements is equal to the assembly of the rigid body modes of the individual elements taking into account the multiplicity of those degrees of freedom that lie in multiple neighboring elements. In the case of asphaltic materials we choose the element stiffness as the property for discrimination between elements. We can think of stones, bitumen, and air voids. We should note that we compute the rigid body modes of each independent body of material. Hence, two bodies of the same material imply 12 deflation vectors. This has a physical meaning also: two bodies will not rotate and translate at the same time and at the same rate. Therefore, these movements need to be taken care of independently.

Acknowledgment. We would like to thank both referees for their thorough review of our paper which contributed to some important improvements of the original manuscript.

REFERENCES

- [1] K. J. BATHE, *Finite Element Procedures*, 2nd revised ed., Prentice Hall, Englewood Cliffs, NJ, 1995.
- [2] M. BOLLHÖFER AND Y. SAAD, *Multilevel preconditioners constructed from inverse-based ILUs*, SIAM J. Sci. Comput., 27 (2006), pp. 1627–1650.
- [3] CAPA3D, *Capa-3d computer aided pavement analysis*, available online at <http://www.capa-3d.org>, 2009.
- [4] A. DRESCHER, N. KRINGOS, AND A. SCARPAS, *On the behavior of a parallel elasto-visco-plastic model for asphaltic materials*, Mech. Mater., 42 (2009), pp. 109–117.
- [5] J. FRANK AND C. VUIK, *On the construction of deflation-based preconditioners*, SIAM J. Sci. Comput., 23 (2001), pp. 442–462.
- [6] G. H. GOLUB AND C. F. VAN LOAN, *Matrix Computations*, 3rd ed., Johns Hopkins University Press, Baltimore, 1996.
- [7] M. GRIEBEL, D. OELTZ, AND M. A. SCHWEITZER, *An algebraic multigrid method for linear elasticity*, SIAM J. Sci. Comput., 25 (2003), pp. 385–407.
- [8] T. JÖNSTHÖVEL, M. VAN GIJZEN, C. VUIK, C. KASBERGEN, AND A. SCARPAS, *Preconditioned conjugate gradient method enhanced by deflation of rigid body modes applied to composite materials*, CMES Comput. Model. Eng. Sci., 47 (2009), pp. 97–118.
- [9] T. B. JÖNSTHÖVEL, M. B. VAN GIJZEN, S. MACLACHLAN, A. SCARPAS, AND C. VUIK, *Comparison of the deflated preconditioned conjugate gradient method and algebraic multigrid for composite materials*, Comput. Mech., 48 (2011), pp. 1–13.
- [10] E. F. KAASSCHIETER, *Preconditioned conjugate gradients for solving singular systems*, J. Comput. Appl. Math., 24 (1988), pp. 265–275.
- [11] A. KLAWONN AND O. B. WIDLUND, *A domain decomposition method with Lagrange multipliers and inexact solvers for linear elasticity*, SIAM J. Sci. Comput., 22 (2000), pp. 1199–1219.
- [12] A. KLAWONN, O. B. WIDLUND, AND D. MAKSYMILIAN, *Dual-primal FETI methods for three-dimensional elliptic problems with heterogeneous coefficients*, SIAM J. Numer. Anal., 40 (2002), pp. 159–179.
- [13] T. LU AND S. SHIOU, *Inverses of 2×2 block matrices*, Comput. Math. Appl., 43 (2002), pp. 119–129.

- [14] R. A. NICOLAIDES, *Deflation of conjugate gradients with applications to boundary value problems*, SIAM J. Numer. Anal., 24 (1987), pp. 355–365.
- [15] J. M. TANG, S. P. MACLACHLAN, R. NABBEN, AND C. VUIK, *A comparison of two-level preconditioners based on multigrid and deflation*, SIAM. J. Matrix Anal. Appl., 31 (2010), pp. 1715–1739.
- [16] J. M. TANG, R. NABBEN, C. VUIK, AND Y. A. ERLANGGA, *Comparison of two-level preconditioners derived from deflation, domain decomposition and multigrid methods*, J. Sci. Comput., 39 (2009), pp. 340–370.
- [17] A. VAN DER SLUIS AND H. A. VAN DER VORST, *The rate of convergence of conjugate gradients*, Numer. Math., 48 (1986), pp. 543–560.
- [18] P. VANĚK, J. MANDEL, AND M. BREZINA, *Algebraic multigrid by smoothed aggregation for second and fourth order elliptic problems*, Computing, 56 (1996), pp. 179–196.